# COUPLED HYGROTHERMAL, ELECTROCHEMICAL, AND MECHANICAL MODELLING FOR DETERIORATION PREDICTION IN REINFORCED CEMENTITIOUS MATERIALS

## A. MICHEL[*], M.R. GEIKER[†], M. LEPECH[††] AND H. STANG[*]

[*] Department of Civil Engineering
Technical University of Denmark (DTU)
2800 Kgs. Lyngby, Denmark
e-mail: almic@byg.dtu.dk, web page: http://www.dtu.dk

[†] Department of Structural Engineering
Norwegian University of Science and Technology (NTNU)
7491 Trondheim, Norway
Email: mette.geiker@ntnu.no, web page: http://www.ntnu.edu

[††] Department of Civil and Environmental Engineering
Stanford University
Stanford, CA 94305, USA
Email: mlepech@stanford.edu, web page: http://www.stanford.edu

**Key words:** Coupled Problems, Multiphysics Problems, Multiscale Problems, Corrosion, Concrete.

**Abstract.** In this paper a coupled hygrothermal, electrochemical, and mechanical modelling approach for the deterioration prediction in cementitious materials is briefly outlined. Deterioration prediction is thereby based on coupled modelling of (*i*) chemical processes including among others transport of heat and matter as well as phase assemblage on the nano and micro scale, (*ii*) corrosion of steel including electrochemical processes at the reinforcement surface, and (*iii*) material performance including corrosion- and load-induced damages on the meso and macro scale. The individual FEM models are fully coupled, *i.e.* information, such as such as corrosion current density, damage state of concrete cover, *etc.*, are constantly exchanged between the models.

## 1 INTRODUCTION

Critical sets of civil infrastructure systems form the foundation for quality of life and enable global development and progress. Consuming vast amounts of material resources and energy, it is essential that global civil infrastructure is designed according to broad, long term design goals for the benefit of our planet and the current and future generations of humans, animals, and plants that will call it home. However, deterioration of civil infrastructure (*e.g.* bridges, tunnels, roads, buildings) together with increasing loads (*e.g.* traffic load, intensity, climate changes, *etc.*) presents a major challenge to achieving these goals in many developed countries [1]. Therefore, the renovation, renewal, and maintenance of existing civil infrastructures is a primary challenge for researchers and practitioners alike. Experience from

the past 20 years has shown that the initial costs of construction are often dwarfed by the costs of repairing, inspecting, and maintaining a civil infrastructure over its useful life [2]. While engineering tools and methods are well developed for the structural design of new structures, tools for assessing current and predicting the future condition of civil infrastructure are less advanced. Existing prediction tools are largely empirical, and thus limited in their ability to predict the performance of new materials, structural, or maintenance solutions. As such, the inability to reliably assess the long-term future ramifications of today's design decisions poses a major obstacle for the design of civil infrastructure. A primary reason for the lack of reliable modelling tools is that deterioration mechanisms are highly complex, involve numerous coupled phenomena that must be evaluated across a range of scales, and often cut across several academic disciplines.

Multi-physics and multi-scale deterioration modelling holds the potential to address these challenges and to enable realistic and reliable long-term performance predictions of civil infrastructure. The basic concept of such a multi-physics and multi-scale modelling framework for reinforced concrete structures is presented in Figure 1. Fundamental, science-based models employed in the modelling framework deal with transport phenomena (moisture, temperature, oxygen, etc.) and phase changes in cementitious materials, electrochemistry (reinforcement corrosion), and fracture mechanics on various length and time scales. These individual science-based models, describing actual physical phenomena, are organized in groups, so-called modules in the modelling framework. To establish a link between the individual modules an interface module is required that allows for passing of information from one module to another, thereby bridging various length and time scales and allowing for concurrent performance simulations of reinforced concrete structures. The interface module may thereby be based on information-passing multi-scale (IPM) methods, thermodynamically constrained internal state variables (ISV), or local enrichment based
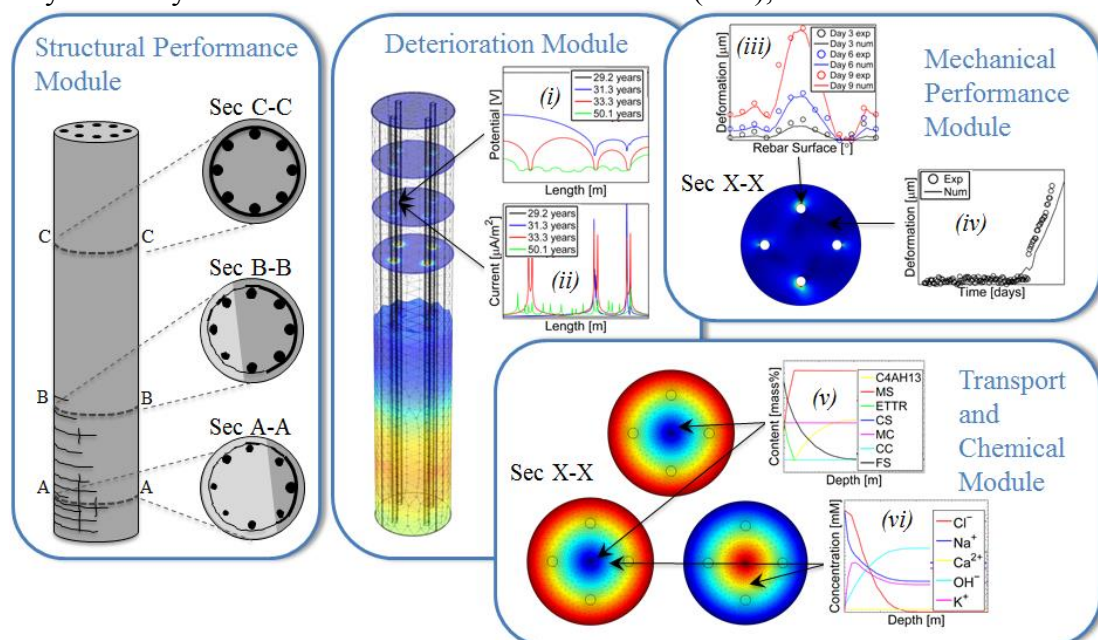


**Figure 1**: Multi-physical and multi-scale modelling framework for deterioration of reinforced concrete, including physical, chemical, electrochemical, and fracture mechanical processes at the material and meso-scale, which are further coupled with mechanical deterioration processes at the structural/component scale, from [3].

concurrent multi-scale (LECM) methods to bridge time and length scales of the individual models describing actual deterioration phenomena in reinforced concrete.

In the following sections of this paper, the theoretical background of the individual modules for reinforced concrete structures suffering from reinforcement corrosion (the leading deterioration mechanism of civil infrastructure built from reinforced concrete destroying more than 3% of the world's GDP [1]) is outlined. Full coupling of physical and chemical processes, mechanical performance, and electrochemical processes on the material scale of the modelling framework is presented. Although not presented in this paper, results of such coupled transport, chemical, and electrochemical processes may be further used for the evaluation of structural performance as well as sustainability of reinforced concrete structures.

## 2 MODELLING HEAT, MOISTURE, AND ION TRANSPORT

Within the 'Transport and Chemical Module', coupled transport of heat and moisture, comprising both liquid and water vapour moisture transport, in porous media is modelled using Richard's equation, while multi-ion species transport and the interaction of predominant ions in the cementitious pore solution with solid phases of hydrated Portland cement is modelled by the Nernst-Planck equation and a thermodynamic model, respectively.

### 2.1 Coupled heat and moisture transport in porous media

Assuming that contributions due to air transfer, gravity, radiation, liquid transport due to temperature gradients, and effects of the gaseous phase on the moisture and heat storage are negligible as well as temperatures remain below the boiling temperature of water [4], coupled heat moisture transport in porous media may be described as follows

$$\rho C \frac{\partial T}{\partial t} = \nabla \big( k_{T,T} \nabla T + k_{T,pC} \nabla pC \big)$$

$$\frac{\partial \theta_l}{\partial p_c} \frac{\partial p_c}{\partial pC} = C_{pC} \frac{\partial pC}{\partial t} = \nabla \big( k_{pC,pC} \nabla pC + k_{pC,T} \nabla T \big)$$

(1)

where $\rho$ is the mass density of concrete, $C$ the specific heat capacity of concrete, $T$ the temperature, $t$ the time, $pC$ the logarithm of the capillary pressure, $\theta_l$ the moisture content, $pc$ the capillary pressure, $C_{pC}$ the moisture capacity and $k$ transport coefficients for the heat, $T$, and moisture transfer, $pC$, respectively. For the solution of the coupled partial differential equations, material specific information on the various transport coefficients ($k$), capillary pressure curve ($\theta_{pc}$) describing the moisture storage, and boundary conditions are needed. The various transport coefficients of Eq. 1 may be described as follows

$$k_{T,T} = \lambda$$

$$k_{T,pC} = -l_{lv} \frac{D_v(\Theta_l)}{R_v T} \frac{p_{v,sat} \varphi}{\rho_l R_v T} \frac{\partial p_c}{\partial pC}$$

(2)

$$k_{pC,pC} = -K_l(\Theta_l) \frac{\partial p_c}{\partial pC} - \frac{D_v(\Theta_l)}{R_v T} \frac{p_{v,sat} \varphi}{\rho_l R_v T} \frac{\partial p_c}{\partial pC}$$

$$k_{pC,T} = \frac{D_v(\Theta_l)}{R_v T} \frac{p_{v,sat}\varphi}{\rho_l R_v T} \frac{\partial p_{v,sat}}{\partial T}$$

where $\lambda$ is the thermal conductivity, $l_{lv}$ the specific latent heat of evaporation, $D_v(\theta_l)$ the moisture dependent vapour diffusion coefficient, $R_v$ the gas constant of water vapour, $p_{v,sat}$ the saturation vapour pressure, $\rho_l$ the density of water, $\varphi$ the relative humidity and $K_l(\theta_l)$ the liquid conductivity coefficient. The moisture dependent vapour diffusion coefficient, $D_v(\theta_l)$, and the liquid conductivity coefficient, $K_l(\theta_l)$, may be described through a mechanistic modelling approach, see *e.g.*, [5] and [6]. This mechanistic modelling approach considers thereby the microstructure of the porous media. To describe the moisture storage behaviour of porous media, a bimodal function of van Genuchten type may be used, see *e.g.*, [7], which can be given as follows

$$\Theta_{p_c} = \Theta_{cap} \sum_{i=1}^{k} \frac{l_i}{(1 + (a_i p_c)^{n_i})^{m_i}} \tag{3}$$

where $\theta_{cap}$ is the capillary moisture content, $a_i$, $n_i$, and $m_i$ are shape parameters and $l_i$ a weighting factor.

## 2.2 Multi-ion transport in porous media

The transport of ions in porous media is mainly governed by three different transport phenomena, *i.e.* diffusion, migration, and convection. Nernst-Planck equation allows for the description of multi-ion transport in porous media taking into account these transport phenomena and may be given as follows

$$\frac{\partial c_i}{\partial t} = \nabla\big(D_i \nabla c_i + z_i u_{m,i} F c_i \nabla E - c_i v\big) \tag{4}$$

where $c_i$ is the ionic concentration, $D_i$ the ionic diffusion coefficient, $z_i$ the charge number of the ionic species, $u_{m,i}$ the ionic mobility, $F$ Faraday's constant, $E$ the electrostatic potential and $v$ the velocity of the solvent. To account for the impact of moisture on the diffusion of ions the relation proposed in [8] may be used
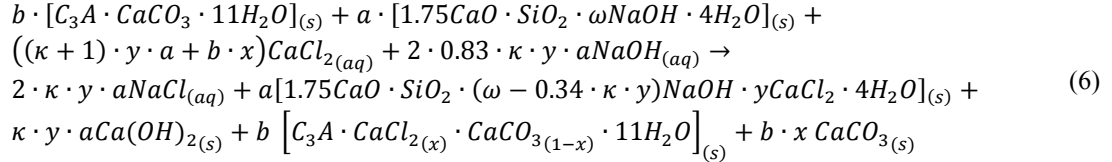
$$D_i(S_l) = D_i^0 S_l^{\xi} \tag{5}$$

where $D_i^0$ is the free ionic diffusion coefficient in bulk water, $S_l$ the degree of saturation and $\xi$ a model parameter.

## 2.3 Phase assemblage in hydrated Portland cement

Ions are known to be physically adsorbed and/or chemically bound in porous media, such as concrete, commonly referred to as binding. The bound ions will not participate further in the ingress. With respect to reinforcement corrosion, especially the binding process of chloride ions is of interest as only free chloride ions may initiate reinforcement corrosion. Among others, chloride binding in hydrated Portland cement may be described through thermodynamic modelling for the phase equilibria based on the application of the phase rule as proposed in *e.g.* [9] and [10]. Calculations assume thermodynamically stable or metastable equilibrium at constant temperature and pressure, and therefore strict observance with the phase rule. While the overall reaction scheme for chloride binding in hydrated Portland

cement considering the total content of alkalis can be found [9] and [10], as an example the equations for chloride binding in Portland cement pastes in which Na is still present in the C-S-H and no AFm (alumina, ferric oxide, monosulfate) phases other than monocarbonate are present may be described as follows

$$
\begin{aligned}
&b \cdot [C_3A \cdot CaCO_3 \cdot 11H_2O]_{(s)} + a \cdot [1.75CaO \cdot SiO_2 \cdot \omega NaOH \cdot 4H_2O]_{(s)} + \\
&((\kappa + 1) \cdot y \cdot a + b \cdot x)CaCl_{2(aq)} + 2 \cdot 0.83 \cdot \kappa \cdot y \cdot aNaOH_{(aq)} \rightarrow \\
&2 \cdot \kappa \cdot y \cdot aNaCl_{(aq)} + a[1.75CaO \cdot SiO_2 \cdot (\omega - 0.34 \cdot \kappa \cdot y)NaOH \cdot yCaCl_2 \cdot 4H_2O]_{(s)} + \\
&\kappa \cdot y \cdot aCa(OH)_{2(s)} + b \left[ C_3A \cdot CaCl_{2(x)} \cdot CaCO_{3(1-x)} \cdot 11H_2O \right]_{(s)} + b \cdot x \, CaCO_{3(s)}
\end{aligned}
\tag{6}
$$

where $a$ is the content of C-S-H, $b$ the initial content of monocarbonate, $\omega$ the molar ratio of NaOH between chloride-free C-S-H and C-S-H, $m$ the fraction of Friedel's salt in the solid solution phase at the chloride content where all alkalis have been released to the pore solution from the C-S-H, $x$ the fraction of Friedel's salt in the AFm solid solution phase, $y$ the content of $CaCl_2$ in the C-S-H, the relation between $y$ and $x$ may be described as follows

$$
\begin{aligned}
y &= 0.0601x^2 + 0.0164x \quad \text{for white Portland cement} \\
y &= 0.0376x^2 + 0.0064x \quad \text{for gray Portland cement}
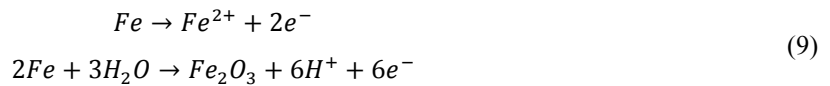\end{aligned}
\tag{7}
$$

where $\kappa$ is defined as

$$
\kappa = \omega(PS/a)\, 0.2354
\tag{8}
$$

where $PS$ is the amount of solution in millilitre.

## 3 MODELLING REINFORCEMENT CORROSION

Within the 'Deterioration Module' (see Figure 1), electrochemical processes describing corrosion of reinforcement in concrete structures is dealt with. It is thereby assumed that corrosion of reinforcement in concrete can be described by the same electrochemical processes as the corrosion of a metal in an electrolyte [11]. An overview of fundamental electrochemical and physical processes describing the corrosion of steel in concrete is given in Figure 2 as proposed in [12]. Two electrochemical half-cell reactions must take place at the metal surface for corrosion to occur, the anodic (oxidation) and the cathodic (reduction) half-cell reaction. The anodic half-cell reaction is characterised by liberating electrons, which are consumed in the cathodic half-cell reaction. The electrons liberated at the anode are conducted through the metal to the cathode and the electrical circuit is then closed by an ionic exchange current through the concrete. Typical anodic reactions, such as the oxidation of iron are given in Eq. 12, while common cathodic reactions, such as e.g. the reduction of oxygen are presented in Eq. 13, see *e.g.*, [12].

$$
\begin{aligned}
Fe &\rightarrow Fe^{2+} + 2e^- \\
2Fe + 3H_2O &\rightarrow Fe_2O_3 + 6H^+ + 6e^-
\end{aligned}
\tag{9}
$$

$$
\begin{aligned}
O_2 + 4H^+ + 4e^- &\rightarrow 2H_2O \\
O_2 + 2H_2O + 4e^- &\rightarrow 4OH^-
\end{aligned}
\tag{10}
$$

However, depending on the potential and pH at the steel surface, other cathodic reactions, such as the reduction of hydrogen or water, may take place. A detailed overview of thermodynamically feasible anodic and cathodic reactions associated with reinforcement

corrosion can be found in *e.g.* [12]. Thus, for a thorough description of the reinforcement corrosion process, thermodynamics and kinetics must be considered as well as their dependence on other parameters such as *e.g.* temperature, moisture, oxygen, *etc*.
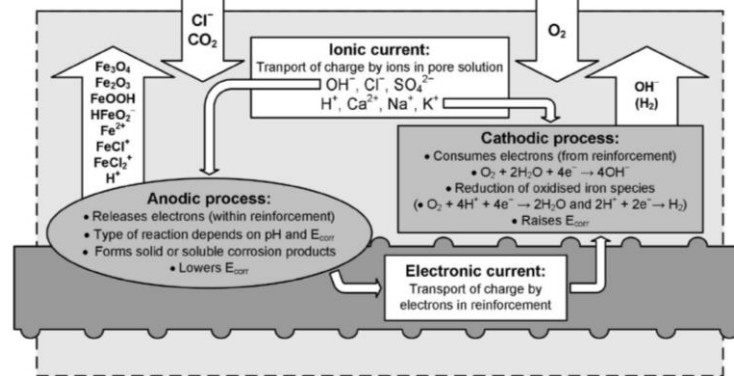


**Figure 2**: Overview of electrochemical and physical processes describing corrosion in concrete, from [12].

## 3.1 Corrosion potential and corrosion current density distribution

Two equations may be used to describe the electrochemical processes in the concrete pore solution acting as electrolyte [13]. The first one is Laplace's equation, which describes the potential distribution in an electrolyte assuming electrical charge conservation and isotropic conductivity.

$$\nabla^2 E = 0 \tag{11}$$

The second is Ohm´s law, which may be used to determine the rate of dissolution of iron at any point on the steel surface in concrete if the potential distribution around that point and the resistivity, $\rho_{conc}$, of the electrolyte is known [14].

$$i_{corr} = -\frac{1}{\rho_{conc}}\frac{\partial E}{\partial n} \tag{12}$$

## 3.2 Thermodynamics of reinforcement corrosion

Among others, thermodynamics provide the possibility to investigate and assess the likelihood of reactions (in the case of reinforcement corrosion: anodic and cathodic half-cell reactions) to occur under certain conditions. To describe the equilibrium potentials, $E_0$, of thermodynamically feasible half-cell reactions for the corrosion process, Nernst equation can be used, which may be written as follows (Perez 2004)

$$E_0 = E_0^0 - \frac{RT}{zF}ln\left(\frac{\alpha_{Red/Ox}}{\alpha_{Ox/Red}}\right) \tag{13}$$

where $E_0^{0}$ is the standard equilibrium potential, $R$ the gas constant, and $\alpha_{Red/Ox}$ the chemical activity of the reductant and oxidant, respectively. Nernst equation may be further used to construct pH - potential diagrams, or more frequently called Pourbaix diagrams, providing a graphical overview of thermodynamically favoured reactions (*i.e.* reactions with a negative free enthalpy) as a function of the pH and the half-cell potential. The Pourbaix diagram for iron in chloride ion containing water (commonly used to investigate corrosion reactions of steel in concrete [12]) is illustrated in Figure 3. In combination with the information from the

'Transport and Chemical Module', the pH in the concrete pore solution can be determined. Along with the electric potential, determined from Laplace equation, thermodynamically feasible anodic and cathodic reactions can then be selected when modelling reinforcement corrosion processes.
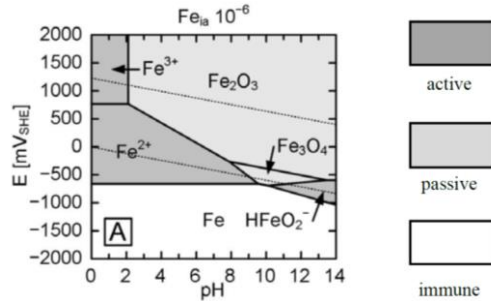


**Figure 3**: Pourbaix diagram for Fe-Cl-$H_2O$ system at 25°C, with an Fe ion activity of $10^{-6}$ mol/L and Cl concentration of 0.035 mg/L, after [12].

## 3.3 Kinetics of reinforcement corrosion

Although thermodynamics provide means to assess the possibility of corrosion reactions to occur under various conditions, no information on the rate of these reactions is obtained. Therefore, the kinetics of electrochemical reactions must be considered to fully assess the corrosion mechanism. Once corrosion is initiated, the potentials of the half-cell reactions on the steel surface are shifted from their equilibrium potentials and a (corrosion) current will start to flow. The shift from the equilibrium potential is known as polarisation and the kinetics of the electrochemical half-cell reactions are governed by the degree of polarisation. A measure for the polarisation is the overpotential, $\eta$, which is the difference between the half-cell potential, $E_{c/a}$, and the equilibrium potential, $E_{0a/0c}$. Information on the polarisation of electrodes (anode and cathode) can be summarised in so-called Evan's diagrams relating the half-cell potential to the corrosion current. The Evan's diagram for the anodic and cathodic half-cell reactions assuming the formation of $Fe^{2+}$ at the anode and $OH^-$ at the cathode is given in Figure 4. The corrosion potential (also referred to as mixed potential), $E_{corr}$, and the corrosion current density, $i_{corr}$, can be determined from the intersection of the anodic and the cathodic polarisation curve. The relation between the corrosion current and the half-cell potential may be described by the Butler-Volmer equation assuming that the kinetics are governed by activation, concentration, and resistance polarisation and that the electrochemical reactions take place at separate electrodes and the polarisation is high [15].

$$i = i_0 exp(\Psi) \ with \ \Psi = ln(10)\frac{E - E_0}{b_T} \tag{14}$$

where $i$ is the corrosion current density, $i_0$ the exchange current density, and $b_T$ the Tafel constant, which is defined as follows

$$b_T = ln(10)\frac{RT}{\alpha z F} \tag{15}$$

where $\alpha$ is the symmetry factor. To include the effects of concentration polarisation on the relation between the half-cell potential and the corrosion current density, Eq. 18 may be extended and written as follows [16]

351

$$i = i_0 exp\left(\frac{1-\Psi}{1+i_0/i_{lim}\Psi}\right) \quad (16)$$

where $i_{lim}$ is the limiting corrosion current density, which may be defined as follows [17]

$$i_{lim} = \frac{zFD_{O2}}{\delta}c_{O2} \quad (17)$$

where $D_{O2}$ is the oxygen diffusion coefficient, $c_{O2}$ the oxygen concentration at the electrode surface and $\delta$ the diffusion layer thickness. A number of factors influence the shape of the polarisation curve, which in turn governs the kinetics of the corrosion process. Among others, the surface state of the electrode, temperature, moisture content, and geometry are decisive for the overpotential at the anode and cathode [17]. For example, the temperature, moisture content, and geometry are important parameters for diffusion-controlled corrosion. A high moisture content considerably hinders the oxygen transport from the concrete surface to the electrode. This may lead to a depletion of oxygen at the cathode ceasing the cathodic half-cell reaction (assuming reduction of oxygen as governing half-cell reaction) and subsequently the corrosion process itself. Furthermore, several electrochemical parameters, such as the exchange current density or the equilibrium potential are influenced by temperature. This highlights the importance of a fully coupled modelling framework, i.e. coupling between mass and heat transport, phase assemblage, and kinetics and thermodynamics of reinforcement corrosion, for a reliable and realistic assessment as well as long term prediction of the performance of reinforced concrete structures with respect to corrosion.
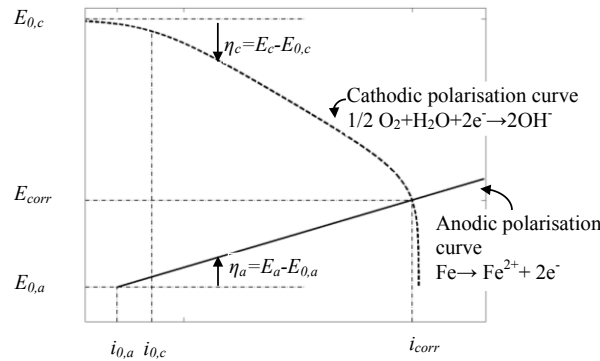


**Figure 4**: Evan's diagram illustrating the anodic and cathodic polarisation on the steel surface, after [18].

### 3.4 Initiation of reinforcement corrosion

To link corrosion initiation, *i.e.* the formation of anodic regions at the reinforcement surface, and propagation of reinforcement corrosion a conditional statement may be defined along the reinforcement surface. In case of chloride-induced corrosion, the conditional statement may comprise the definition of a critical chloride threshold for elements along the reinforcement surface, which might be defined as follows

$$BC_{Steel} = \begin{cases} i_a \\ i_c \end{cases} for \begin{array}{c} c_{cl} \geq c_{crit} \\ c_{cl} < c_{crit} \end{array} \quad (18)$$

where $BC_{Steel}$ is the boundary condition along the steel surface, $i_a$ the anodic polarisation curve, $i_c$ the cathodic polarisation curve, $c_{cl}$ the chloride concentration along the

reinforcement, and $c_{crit}$ the critical chloride threshold defined along the reinforcement. As an approximation $c_{cl}$ may be varied randomly along the reinforcement surface to account for the influence of various parameters and represent a realistic reinforced concrete structure with defects, voids, *etc.* present at the concrete steel interface [19].

## 4 CORROSION-INDUCED CONRETE DAMAGE

Once corrosion is initiated, electrochemical half-cell reactions are taking place along the reinforcement. The ionic reaction products of these half-cell reactions may further react and form solid corrosion products in the vicinity of the reinforcement. The type of corrosion products formed; depend thereby on the thermodynamic conditions present in the vicinity of the reinforcement [12]. Independent of the type of iron oxides formed as a result of active corrosion, the iron oxides occupy a larger volume than the initial iron that is consumed during the corrosion reaction, see *e.g.,* [20]. The increased volume of corrosion products causes tensile stresses in the surrounding concrete and may lead to concrete cracking, spalling, or delamination if the tensile strength of the concrete is exceeded. This damage process is described in the 'Mechanical Performance Module', which utilizes a thermal analogy to model the expansive nature of solid corrosion products and corrosion-induced damage, see Figure 5. The developed fracture mechanics model, furthermore, accounts for the penetration of solid corrosion products into the available pore space of the surrounding cementitious material, as well as non-uniform distribution of corrosion products around the circumference of the reinforcement, see e.g. [21]. Faraday´s law is used to relate the cross sectional reduction per time unit to the corrosion current density 'Deterioration Module'.
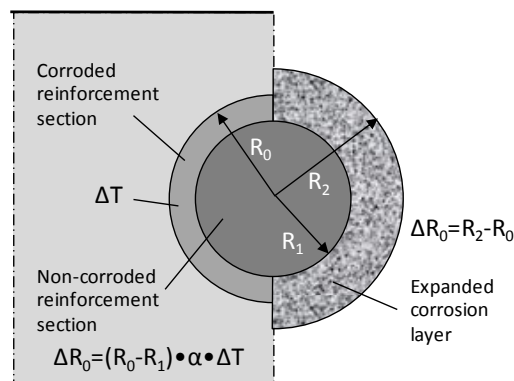


**Figure 5**: General modelling approach for corrosion-induced damage in concrete including load application and geometrical considerations, from [22].

### 4.1 Coupled lattice and FEM model

To simulate corrosion-induced damage in concrete, a random, triangular lattice of truss elements is chosen within the present framework. As the formation of cracks is assumed to take place only in the concrete domain, the remaining domains (steel and corrosion layer) are modelled with continuum elements. The random lattice of truss elements in the concrete domain is established by initially creating a regular square lattice in the concrete domain. Within each cell of the regular lattice, a point is selected at random with uniform distribution. Subsequently, Voronoi construction is used to create a random lattice by connecting the three points that are closest to each other. The randomness of the lattice can be varied through the

introduction of a sub-cell in the square lattice, from which the random point is chosen.

Crack formation and growth within the concrete domain is achieved by removing the element with the highest stress to tensile strength ratio and greater than unity. Upon the next loading step the updated system of equations is recomputed and the analysis repeated until the system fails. This step-by-step removal of lattice elements allows for crack evolution in the specimen and for tracking of microcrack propagation and crack pattern in the simulation. To determine the nodal displacements and subsequently the stresses in the elements of the lattice for each analysis step an elastic analysis is performed. 2-D nodal displacements can thereby be obtained as follows for a set of linear equations within a FEM formulation

$$\{F\} = [K]\{U\} \tag{19}$$

where $F$ is the global nodal force vector, $K$ the global stiffness matrix, and $U$ the global nodal displacement vector. The global stiffness matrix is hereby obtained as follows

$$[K] = \int [B^T][D][B]h d\Omega \tag{20}$$

where $B$ is the strain matrix, $D$ the constitutive material matrix, and $h$ the thickness of the domain, $\Omega$. In the present modelling approach, lattice and continuum elements are combined to discretize the various domains of the model, *i.e.* the concrete domain is discretized using truss elements while the corrosion product and reinforcement domain are discretized using bilinear quadrilateral and linear triangular elements, respectively. The thermal analogy to mimic the expansive nature of corrosion products is implemented by equivalent nodal forces, $f_{cp,t}$, for the corrosion product domain, $cp$, which can be determined as follows

$$[f_{cp,t}] = \int_{A_{cp}} [B_{cp}^T][D_{cp}][\varepsilon_{cp,t}]h dA_{cp} \tag{21}$$

in which the thermal strain matrix, $\varepsilon_{cp,t}$, may be given as follows for 2-D

$$[\varepsilon_{cp,t}] = \begin{bmatrix} \alpha\Delta T \\ \alpha\Delta T \\ 0 \end{bmatrix} \tag{22}$$

The modelling approach is formulated in Matlab[®], and focus was placed on efficient algorithms to allow for simulations with large numbers of degrees of freedom (DOFs), *i.e.* tens of thousands of elements. To solve the set of linear equations (see Eq. 19) and ensure convergence of the solution, an iterative conjugate gradients squared method solver is used. Finally, it should be noted that the simulation of the corrosion process is time dependent, *i.e.* the corrosion product domain is growing. This requires reassembly of the corrosion product and steel domain for every 'time step'. To account for the corrosion-induced damage from one 'time step' to another, an internal nodal force vector is created for each time step, which assures that corrosion-induced damage is transferred from the previous 'time step'. The internal nodal force vector, $f_i$, can be calculated as follows

$$[f_i] = \int_A [B^T][\sigma]h dA \tag{23}$$

where $\sigma$ is the element stress.

## 5   SUMMARY AND CONCLUSIONS

In this paper, the theoretical background and coupling of chemical, electrochemical, and fracture mechanical processes on different length and time scales in reinforced concrete within a cross disciplinary modelling framework was presented. The presented multi-physics and multi-scale model for corrosion in reinforced concrete structures deals with (*i*) the transport of heat and matter as well as phase assemblage in hydrated Portland cement, (*ii*) corrosion of reinforcement, and (*iii*) material performance including corrosion-induced damages on the meso and macro scale. The modelling framework presented is fully coupled, *i.e.* information, such as phase equilibria, moisture distribution, corrosion rate, damage state of concrete cover, *etc.*, are constantly exchanged between the modules, see Figure 1.

Outcomes of the fully coupled mechanical performance, deterioration, and transport and chemical modules described within this paper may be used for further analysis and coupling within a structural performance module, see Figure 1. In particular, cross sectional reduction of reinforcement due to corrosion and concrete cover damage may be used within such a structural performance module to determine (*i*) structural performance of deteriorated concrete members, (*ii*) change in reinforcement bond strength due to formation of oxidation products, (*iii*) reduction in capacity of corroded reinforcing bars, (*iv*) reduction in ductility of corroded reinforcing bars, *etc.* to assess the structural effects of reinforcement corrosion on concrete structures. Exchange of information between the modules is thereby realized through an 'Interface Module'. Ultimately, such an 'Interface Module' may be built in a standardized manner to allow for future extensions, *e.g.* inclusion of additional deterioration mechanisms such as freeze thaw, alkali silica reaction, of the outlined multi-physics and multi-scale modelling framework. Integration of a standardized 'Interface Module' within the modelling framework will furthermore allow for adaptation of level of detailing relevant for individual cases as well as enable continuously updating based on new knowledge and to identify further research needs.

### REFERENCES

[1]   Koch, G.H., Brongers, M.P.H., Thompson, N.G., Virmani Y.P. and Payer, J.H. *Corrosion Cost and Preventive Strategies in the United States*, Report FHWA-RD-01-156, (2002).

[2]   Lepech, M.D., Geiker M. and Stang, H. Probabilistic design and management of environmentally sustainable repair and rehabilitation of reinforced concrete. *Cem. Concr. Comp.* (2014) **47**:19-31.

[3]   Michel, A, Stang, H., Lepech, M. and Geiker, M.R. Multi-physics and multi-scale deterioration modelling of reinforced concrete, *Key Eng. Mat.* (2016) **665**:13-16.

[4]   Janssen, H., Blocken, B. and Carmeliet, J. Conservative modelling of the moisture and heat transfer in building components under atmospheric excitation, *Int. J. Heat. Mass. Transf.* (2007) **50**:1128-1140.

[5]   Scheffler, G.A. *Validation of hygrothermal material modelling under consideration of the hysteresis of moisture storage*, Ph.D. thesis, Technical University of Dresden, Dresden, Germany, (2009).

[6]   Scheffler, G.A. and Plagge, R. A whole range hygric material model: Modelling liquid and vapour transport properties in porous media, *Int. J. Heat. Mass. Transf.* (2010) **53**:286-296.

[7]   Carmeliet, J. and Roels, S. Determination of the moisture capacity of porous building materials, *J. Build. Phys.* (2002) **25**:209-237.

[8]   Buchwald, A. Determination of the ion diffusion coefficient in moisture and salt loaded masonry materials by impedance spectroscopy, In: *Proceedings of 3rd International PhD Symposium*, Vienna, (2000).

[9]   Nielsen, E.P. *The durability of white Portland cement to chemical attack*, Ph.D. thesis, Technical University of Denmark, Kgs. Lyngby, Denmark, (2004).

[10]  Geiker, M., Nielsen, E.P. and Herfort, D. Prediction of chloride ingress and binding in cement paste, *Mater. Struct.* (2007) **40**:405-417.

[11]  Schießl, P. (Ed.) *Corrosion of steel in concrete*, Report of the Technical Committee 60 CSC, RILEM, Chapman and Hall, (1988).

[12]  Küter, A. *Management of reinforcement corrosion: a thermodynamical approach*, Ph.D. thesis, Technical University of Denmark, Kgs. Lyngby, Denmark, (2015).

[13]  Warkus, J., Raupach, M. and Gulikers, J. Numerical modeling of corrosion - Theoretical backgrounds -, *Mater. Corros.* (2006) **57**: 614-617.

[14]  Isgor, B.O. & Razaqpur, G.A. Modelling steel corrosion in concrete structures, *Mater. Struct.* (2006) **39**:291-302.

[15]  Stern, M. and Geary, A.L. Electrochemical polarization I. A theoretical analysis of the shape of polarization curves, *J. Electrochem. Soc.* (1957) **104**:56-63.

[16]  Böhni, H. *Corrosion in reinforced concrete structures*, Woodhead Publishing Ltd., (2005).

[17]  Bardal, E. *Corrosion and Protection*, Springer-Verlag, London, UK, (2004).

[18]  Martín-Pérez, B. *Service Life Modelling of R.C. Highway Structures Exposed to Chlorides*, Ph.D. thesis, University of Toronto, Toronto, Canada, (1999).

[19]  Angst U.M., Geiker, M.R., Michel, A. et al. The steel–concrete interface, *Mater. Struct.* (2017) **50**:143.

[20]  Marcotte, T. and Hansson, C. Corrosion products that form on steel within cement paste, *Mater. Struct.* (2007) **40**:325-340.

[21]  Thybo, A.E.A., Michel, A. and Stang, H. Smeared crack modelling approach for corrosion-induced concrete damage, *Mater. Struct.* (2017) **50**:146.

[22]  Michel, A., Solgaard, A.O.S., Geiker, M., Stang, H. and Olesen, J.F. Modeling Formation of Cracks in Concrete Cover due to Reinforcement Corrosion. *In Oh, B.H., Choi, O.C. and Chung, L. (Eds) Proceedings of FraMCoS-7*, (2010) pp.944-951.